Dentomaxillofacial Radiology (2020) 49, 20190385

birpublications.org/dmfr

RESEARCH ARTICLE

Evaluation of metal artefacts for two CBCT devices with a new dental arch phantom

[1]Luciano Augusto Cano Martins, [1]Polyane Mazucatto Queiroz, [1]Yuri Nejaim, [2]Karla de Faria Vasconcelos, [3]Francisco Carlos Groppo and [1]Francisco Haiter-Neto

[1]Department of Oral Diagnosis, Division of Oral Radiology, Piracicaba Dental School, University of Campinas (UNICAMP), Sao Paulo, Brazil; [2]Department of Imaging & Pathology, Faculty of Medicine, KU Leuven and Oral and Maxillofacial Surgery, University Hospitals Leuven, Leuven, Belgium; [3]Department of Physiological Sciences, Division of Pharmacology, Piracicaba Dental School, University of Campinas (UNICAMP), Campinas, Brazil

Objectives: To create a new phantom design to evaluate the real impact of artefacts caused by titanium on bone structures in cone beam CT images considering different positions and quantity of metals in the dental arch, with and without metal artefact reduction (MAR).
Methods: A three cylindrical polymethyl methacrylate (PMMA) plate phantom was designed containing eight perforations arranged to simulate the lower dental arch in the intermediate plate. Three titanium cylinders were positioned in different locations and quantities to test different clinical conditions and to quantify the impact of the metal artefact around five bone cylinders. Scans were carried out in seven different protocols (Control, A-F) in two cone beam CT devices (OP300 Maxio and Picasso Trio). Eight regions of interest around each cortical and trabecular bone were used to measure the grey value standard deviation corresponding the artefact expression in the Image J software. Both the artefact expression and the MAR effect were assessed using the Wilcoxon, Friedman (Dunn) and Kruskal–Wallis tests (significance level of 5%).
Results: For both devices, MAR was statistically efficient only for the protocols E, and F. Protocol F (three metals on the adjacent area of the analysis region) showed higher artefact expression when compared to the others.
Conclusion: In conclusion, the new phantom design allowed the quantification of the metal artefact expression caused by titanium. The metal artefact expression is higher when more metal objects are positioned in the adjacent bone structures. MAR may not be effective to reduce artefact expression on the adjacencies of those objects for the devices studied.
Dentomaxillofacial Radiology (2020) **49**, 20190385. doi: 10.1259/dmfr.20190385

Cite this article as: Martins LAC, Queiroz PM, Nejaim Y, Vasconcelos KF, Groppo FC, Haiter-Neto F. Evaluation of metal artefacts for two CBCT devices with a new dental arch phantom. 2020; **49**: 20190385.

Keywords: Artefacts; Cone-Beam Computed Tomography; Dental Implants

Introduction

In the last decades, dental implants have been used in dentistry as an alternative in dental rehabilitation of partially or totally edentulous patients. Surgical planning is carried out by a meticulous clinical inspection and image examinations. Images acquired by cone beam CT (CBCT) is being widely used for more accurate quantification and bone quality evaluation.[1–3] In this image modality, the volumetric projections are reconstructed from a volume element (voxel) matrix. Each voxel represents a numerical grey value according to the linear attenuation of the structures. Due to the inherent characteristics of the technique, such as geometric and

Correspondence to: Luciano Augusto Cano Martins, E-mail: luciano_cano@hotmail.com

Received 28 September 2019; revised 13 December 2020; accepted 29 February 2020

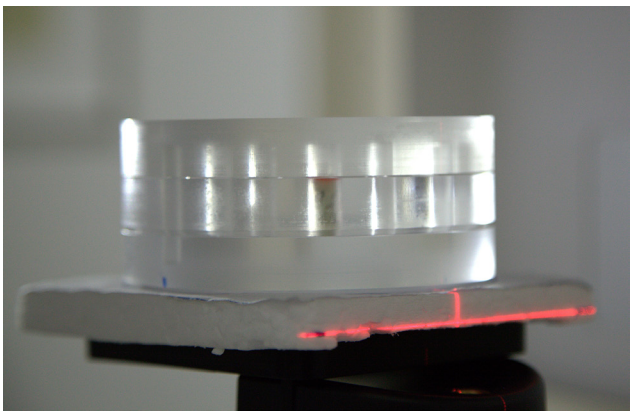

Figure 1 Side-view of the PMMA phantom and plaques in position. PMMA, polymethyl methacrylate.

energy principles and the presence of artefacts, these values have a great variability.[4–6]

Artefacts are structures in the reconstructed image and do not represent the real object.[7] Many aetiologies have been reported and attributed to the CBCT devices, computational reconstruction, patients´ movement and beam hardening.[8–10] The beam hardening phenomenon is one of the most prominent causes of artefacts, and it occurs when lower energy photons are absorbed by high-density materials such as dental implants, metal restorations, and endodontic fillings. This absorption increases the mean energy of the beam, producing streaks and dark bands. Due to this effect, the anatomical interpretation and measurements may be impaired and consequently have a negative influence the implant planning.[11,12]

Strategies have been developed in many CBCT devices to reduce metal artefacts. Mathematical algorithms called metal artefact reduction (MAR) are post-acquisition tools, and they were developed in an attempt to reduce noises caused by the artefacts, by using non-corrupted projections and discarding the projections affected by the artefacts or segmenting the corrupted projections firstly and then replacing using estimated

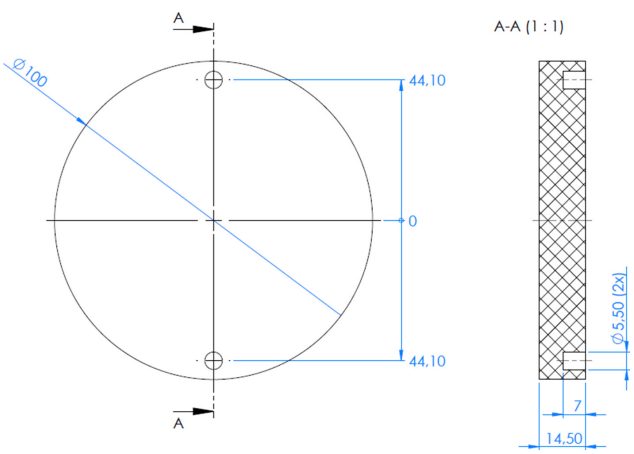

Figure 2 Lower plate schematic drawing.

values.[13–15] The method used to reduce the metal artefact will vary from a manufacturer to another. Thus, the metal artefact production and limitations on the MAR action should be considered when high-density material objects are already present in the dental arch, for this reason, great attention on the placement area and its adjacencies is needed on dental implant planning.[16–18]

In order to investigate the artefacts interference, some authors[2,3,5,10,11,17] have evaluated image quality, measurement accuracy and reliability by means of geometric phantoms, dry skulls and patient image database. Once the X-ray attenuation may vary from a structure or material to another because of their atomic number, the polymethyl methacrylate (PMMA) phantoms are used to create a homogeneous environment, and they are well described in literature.[19–21] Due to its homogeneity, it is possible to quantify the artefact expression by isolating the tissues or the artefacts. Thus, this study aimed to create a new PMMA phantom design to evaluate the impact of artefacts caused by titanium on bone types (cortical and trabecular) in CBCT images considering different positions and quantity of metals in the simulated dental arch, with and without MAR selection. This design may be useful to standardize the quantification of the metal artefact impact when tissue thickness and different materials are being investigated.

Methods and materials

PMMA phantom design

The height of the PMMA phantom was obtained from measuring the height of the maxilla and mandible in occlusion of 10 dry skulls from the anterior nasal spine (anterior point on maxillary bone) and the menton (lowest point on mandibular symphysis). The diameter was obtained by measuring the distances from the lower incisors to the third molars of 10 dry mandibles then all the measurements were averaged (43.5 mm high and 100 mm in diameter). Three cylindrical PMMA plates (100 mm in diameter and 14.5 mm high each) were held overlapping each other by acrylic cylinders (5.5 mm in diameter and 43.5 mm in high) that transfixed all the plates and positioned in the lateral perforations of each plaque (Figure 1).

The lower plate was the phantom base and had only the two lateral perforations 5.5 mm in diameter and 7 mm deep (Figure 2).

The intermediate plate had 10 perforations, 8 simulating the teeth mesiodistal distances of a human lower arch in the region of the first and second molars, first premolars and lateral incisors (Seven 5.5 x 14.5 mm and one 7.5 x 14.5 mm in the first right premolar region). Those distances were obtained from previous studies,[22,23] which evaluated the intermolar, intercanine and mesiodistal coronal distances (Figure 3). The other two perforations were located laterally to transfix the acrylic cylinders that would keep the plaques overlapped in the same position.

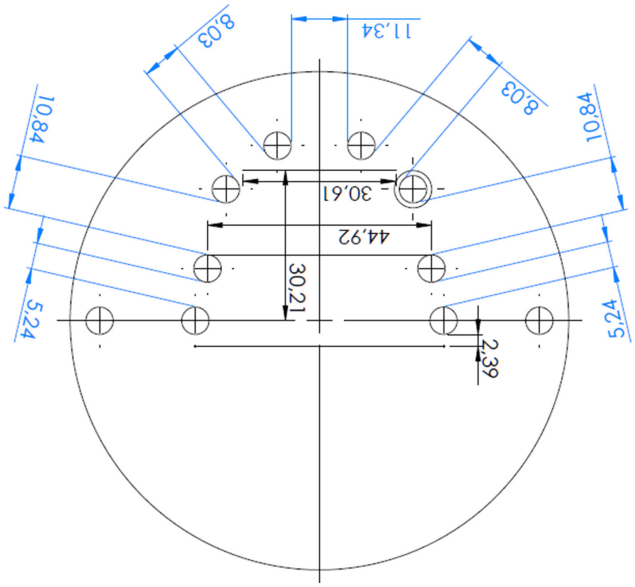

Figure 3 Intermediate plate schematic drawing.

The upper plate had the same perforations of the intermediate but horizontally inverted for the perfect fit between the plates and perforations. All the perforations had a depth of 7.5 mm (Figure 4).

During the image acquisitions, unused perforations were sealed with acrylic cylinders with 5.5 mm in diameter and 22.5 mm high.

Sample preparation

Five bone cylinders (7.5 x 10.5mm) with trabecular and cortical bones from a fresh bovine rib were collected using an 8 mm trephine bur (S.I.N. Implantes, Sao Paulo, Brazil) at 30,000 rpm and abundant saline irrigation by a dentomaxillofacial surgeon (Figure 5A).

In order to simulate a clinical condition, 10 CBCT scans of human mandibles without metallic objects in the arch and with the same parameters used in this study were assessed. The reformatted cross-sections were used to measure the buccal and lingual cortical plates on three portions of the long axis of the first premolar root.

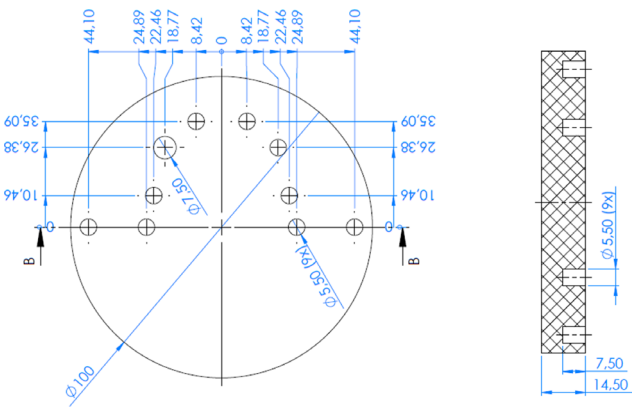

Figure 4 Upper plate schematic drawing.

The mean thickness found was 2 mm, and the cylinders had the cortical bone and diameter adjusted using a cylindrical diamond bur with a high-speed handpiece in abundant saline irrigation. The representative bone cylinders were placed in the perforated space in the intermediate plate of the phantom (the one with 7.5 x 14.5 mm) denominated analysis region (AR).

Titanium cylinders with 14.5 mm in high and 5.5 mm in diameter (S.I.N. Implantes, Sao Paulo, Brazil) (Figure 5B) simulated dental implants. The cylinders were placed at six different positions and quantities in the simulated dental arch, following the acquisition protocols (Table 1). In the protocols A, B and C the titanium cylinders were gradually inserted in the holes located in the opposite side of the arch were the bone cylinder was located considered the AR. In the protocols D, E and F, the titanium cylinders were also gradually inserted in the adjacent side of AR.

CBCT acquisitions

CBCT acquisitions were performed using the OP300 MAXIO (Instumentarium–Tuusula–Finland) and Picasso Trio (Vatech/E-WOO Technology, Seoul, Korea) devices at 90 kVp, 3.2 mA, voxel size 0.2 mm, and field-of-view of 8 × 15 cm and 8.5 × 12 cm, respectively. All five bone cylinders were scanned in the seven protocols with and without the activation of MAR. The algorithms for each device were activated before the acquisitions. The acquisition protocols are shown in Table 1.

The phantom was held in the same position for all acquisition protocols with the use of one custom diagram and the reference lines of the devices. Examples of acquired images are given in Figure 6.

Image analysis

A radiologist examiner assessed all 140 CBCT scans in Image J software (NIH, Bethesda, MD). The long axis of the cylinder determined the axial reconstruction for each bone level. The reformatted sagittal section was used to measure the distances from the endosteal surface plate until the middle point of the cylinder (3.25 mm) for the trabecular level and then 4.25 mm under the middle point the axial reconstruction for the cortical bone level. All the same axial reconstructions were used to measure the average grey value of eight standardized regions of interest (ROIs) positioned around the bone cylinder in the trabecular bone and lower cortical bone levels following the methodology of Queiroz et al[24](Figure 7).

The standard deviation of the eight ROI averages represented the artefact expression around the analysis region in each protocol and then compared to the Control group. Higher SD of grey values represents greater artefact expression and worse image quality. After 30 days, 50% of the images were reevaluated to assess the reproducibility of the method. The other independent variables (metal positions and quantity) were tested to evaluate their influence on the performance of the MAR algorithm.

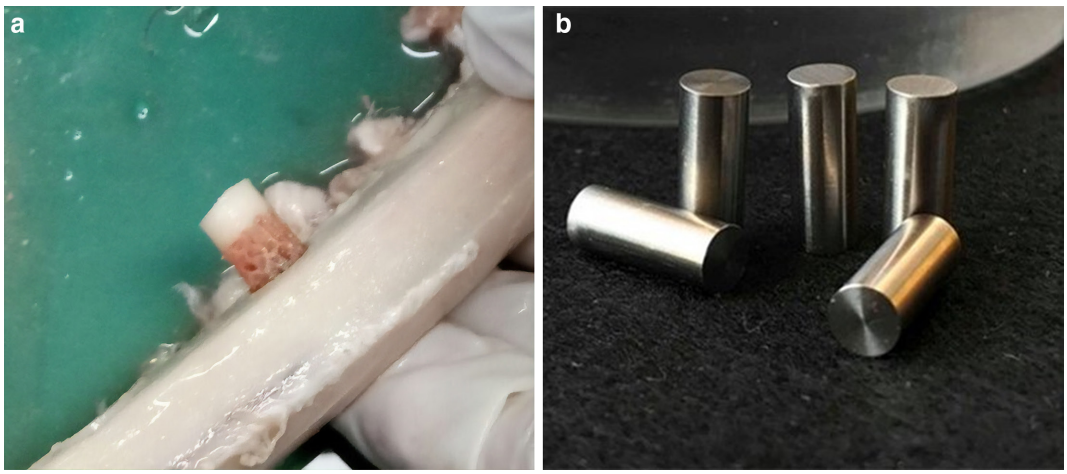

Figure 5 Sample preparation. (A) Bone cylinder removal (B) Titanium cylinders.

Statistical analysis

Shapiro Wilk test was used to observe data distribution. The artefact expression among the devices and protocols was assessed using the Wilcoxon and Kruskal–Wallis (Dunn) tests. The MAR effectiveness was assessed using the Friedman (Dunn) test. The significance level was set at 5% for all tests. All the statistical analyses were carried out using the GraphPad Prism 7.0 (GraphPad Software, La Jolla, CA) and the SPSS 25.0 (SPSS Inc., Chicago, IL).

Results

Picasso Trio ($p < 0.0001$) expressed more artefacts among the protocols independently of the MAR activation. For the protocols, D, E and F, the MAR activation showed significant differences on OP300 Maxio, and for Picasso Trio, the Protocols E and F had significant differences when compared to the other protocols, as shown in Table 2.

The Control group also showed lower artefact expression when compared to the others for both devices. For OP300 Maxio and Picasso Trio, protocol F showed significant higher ($p < 0.0001$) values in comparison with the other protocols, as shown in Figure 8.

When the region around different bone type was analysed (Figure 9) in all protocols it was possible to observe higher values for Picasso Trio ($p < 0.0001$) for cortical bone. In general, it was also observed that the cortical bone expressed more artefacts when compared to the trabecular bone for OP300 Maxio.

Discussion

CBCT acquisition and reconstruction algorithms may vary from a device to another. In the present study, two devices were used (Picasso Trio and OP300 Maxio), and there was a difference identified by the artefact expressions values, which was also confirmed by previous studies using different devices.[6,9,10,19] In addition to the

Table 1 Acquisition protocols, metal positioning and description

	Protocol	*Metal positioning*	*Description*
	Control	AR	No metal
	A	1	One posterior titanium cylinder on the opposite side of the AR
	B	1 and 2	Two posterior titanium cylinders on the opposite side of the AR
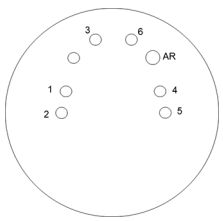	C	1, 2 and 3	Two posterior titanium cylinders and one anteriorly on the opposite side of the AR
	D	4	One posterior titanium cylinders on the adjacent side of the AR
	E	4 and 5	Two posterior titanium cylinders on the adjacent side of the AR
	F	4, 5 and 6	Two posterior titanium cylinders and one anteriorly on the adjacent side of the AR

AR, analysis region.

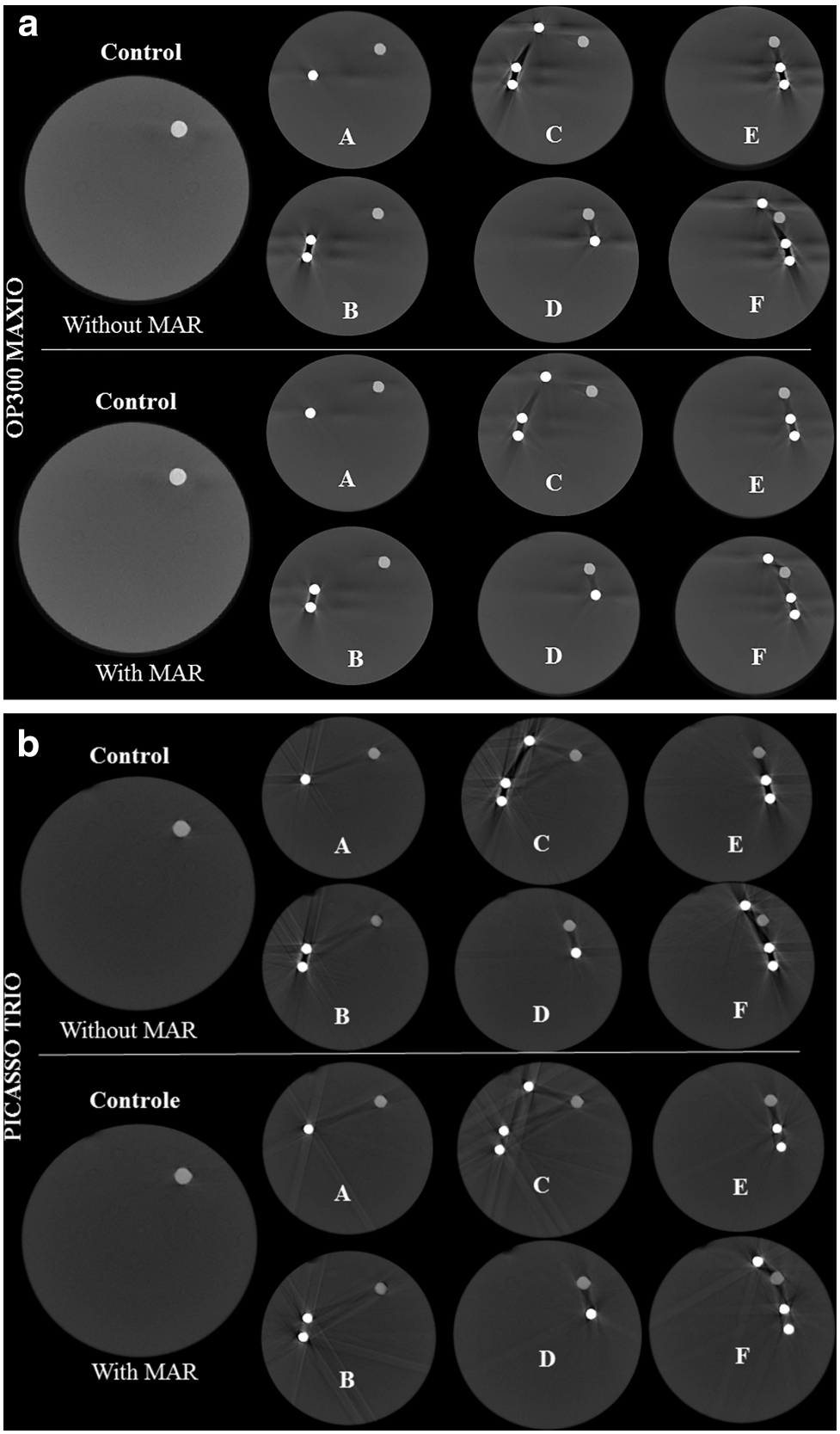

Figure 6 Examples of axial reconstructions (OP300 Maxio (A) and Picasso Trio(B)) without and with the use of MAR in the protocols for a boned sample. MAR, metal artefact rreduction.

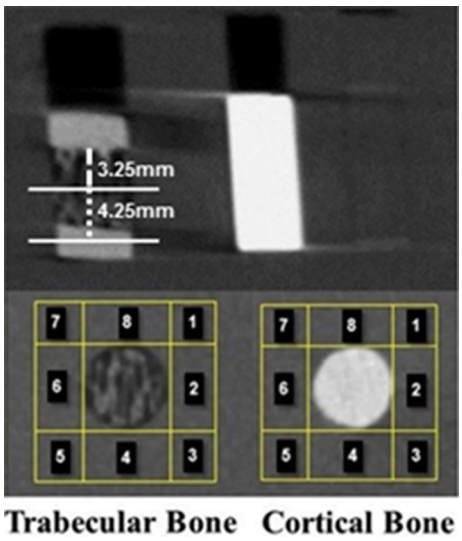

Figure 7 Eight ROIs in axial reconstructions in the vicinity of trabecular and cortical bone.ROI, region of interest.

difference among the devices, the presence of artefacts in the reconstructed image may influence the visualisation of anatomical structures. In the present *in vitro* study, a lower dental arch was simulated in a PMMA phantom, creating a homogeneous and controlled environment making it possible to quantify the artefacts arising from titanium cylinders without other structures attenuation around the tissue or structure that is being analysed. Many previous studies have been conducted using a PMMA phantom for quality assurance phantom in different dimensions.[20] Steiding et al in 2014 have designed a phantom containing five sections and one of them had nine holes (3 x 17.5 mm) for the evaluation of the artefact behavior and also inserted metal objects in different positions.[21] The present study considered the dental distances of the human lower dental arch based on previous studies[22,23] and titanium objects were inserted in different positions of the simulated arch creating clinical scenarios by isolating the artefacts arising from the titanium and its attenuation in the bone types.

Table 2 Mean grey values standard deviation for the image artefact expression for bone with and without MAR in different protocols

	OP300 Maxio		*Picasso Trio*	
Protocol	**With MAR**	**Without MAR**	**With MAR**	**Without MAR**
Control	38 a	37 a	40 ab	39 b
A	38 a	37 a	46 b	45 b
B	39 a	38 a	47 b	47 b
C	47 a	45 a	57 b	54b
D	39 a	43 b	53 c	52 c
E	43 a	53 b	57 b	71 c
F	90 a	136 b	88 a	200 b

Different lowercase letters indicate the statistical difference between MAR activation and without MAR within each protocol.

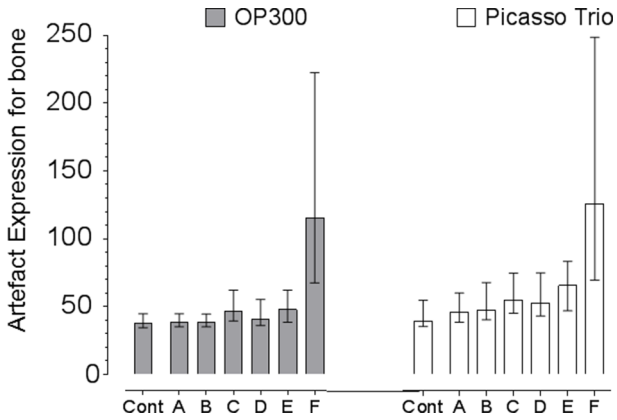

Figure 8 Artefact expression for bone in the protocols.

The X-ray attenuation is different from a structure to another due to their atomic number and the presence of high atomic number materials, such as titanium dental implants. The higher atomic number they have, the more artefact expression may be seen increasing the variability of the grey values, leading to a change of the image contrast and decrease the visualisation of structures.[16] In the present study, a difference in X-ray attenuation was observed in the two bone types studied (trabecular and cortical bone) that were isolated by the bone cylinder in order to simulate an edentulous area before implant placement. Due to its higher mineral density, the cortical bone expressed more artefact when compared to the trabecular bone and it was only observed due the conformity of the present phantom. This reduction in the image quality may decrease the measurement accuracy and the visualisation of neighbouring structures of high-density materials.

The artefact production is not restricted to the area surrounding the generator object only. Previous studies using human mandibles and CBCT images from patients[25–27] have shown that this magnitude is reduced as further from the forming area. It was possible to observe that when the objects were inserted on the

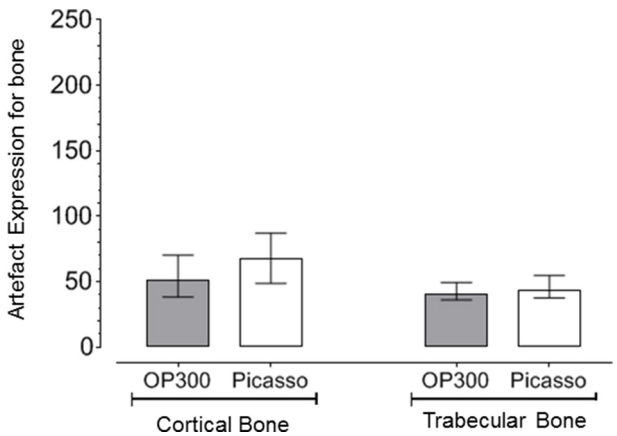

Figure 9 Artefact expression for the cortical and trabecular bone vicinity.

opposite area of the bone cylinders (In the protocols D, E and F), the artefact expression had a minor influence on the grey values for the bone. This finding may be due to the titanium artefact magnitude found by some authors who used titanium (Z = 22) and zirconium (Z = 40) implants.[25,26] These materials have a different atomic number, and the zirconium implants generate more artefact expression than the metallic implants. The present study has only evaluated titanium since this is the most commonly used material and in bone types, once these structures are affected by the artefacts when those objects are already placed in different positions in the arch. We encourage future studies to investigate the effect of the artefacts from other high-density materials in different positions in the dental arch and their attenuation in structures such as teeth. A previous study[27] found differences when the implants were located in the anterior region; the present study showed higher artefact expression on the adjacencies of the analysis region, which is already well known in the literature. Such difference may also be due to the sample selection of the previous study, which consisted of different patients' exams with the different arch format, bone thickness and field of view. This way, the field-of-view (FOV) and energetic parameters used, and the X-ray attenuation may have been different from a patient to another.

The success of an implant depends on bone quality and quantity on the surgical site. This quantification may be carried out by imaging exams such as CBCT and multislice CT. When high-density materials are not in the FOV, CBCT may be used to quantify bone quality but not bone density due to the instability of the grey voxel values scanning parameters and tissue attenuation.[2,5,28] Thus, it may vary from a device to another and the image resolution (partial volume effect). In the present study, the bone samples were affected by the metal artefacts when located in the adjacencies of the titanium cylinder (Protocols D, E and F). This interference may lead to a decrease in bone quality quantification, and consequently may decrease the anatomical visualization and under or overestimate linear bone measurements.[11,12,16,29]

Some alternatives are being studied in order to reduce artefact expression. Acquisition energetic parameters changes such as increasing kVp and activation of MAR tool are ways to reduce noise and improve image quality. This tool may vary from manufacture to another and the methods used. In previous studies,[13–15,30] the algorithm reduced significantly the grey value variability, which represents a greater homogeneity of the image. However, it was not observed in the present study around the bone cylinders when more metal was in the adjacencies for both devices (Protocols A, B and C) which can be attributed to the threshold of activation of the tool. However, MAR showed some positive results when titanium objects are positioned on the opposite area (Protocols D, E and F). These findings should be carefully evaluated when extrapolating the results of an *in-vitro* study on the grey values to a clinical condition because each patient interacts differently with the X-ray beam.

Conclusion

In conclusion, this new PMMA phantom design created a homogeneous environment for the quantification of metal artefact expression related to titanium by simulating a dental arch and using bone cylinders as a tissue reference. The artefact expression is higher when more metal objects are positioned in the adjacent bone structures in CBCT images. The MAR may not be useful to reduce artefact expression for both devices when more titanium objects are placed on the adjacencies of the bone. The effectiveness of the algorithm may vary from a device to another.

Acknowledgment

This study was financed in part by the Coordenação de Aperfeiçoamento de Pessoal de Nível Superior–Brazil (CAPES)–Finance Code 001. Also, we would like to thank the Nice Group Brazil (Limeira, Sao Paulo Brazil) for manufacturing the PMMA phantom and S.I.N. Implantes (Sao Paulo, Sao Paulo, Brazil) for providing the Titanium cylinders and the Trephine bur for the present research.

REFERENCES

1. Leung CKK, Pow EHN, Li TKL, Lo ECM, Chow TW. Accuracy of radiographic measurements for implant planning using cone-beam and helical computer tomography. *J Investig Clin Dent* 2017; **8**: e12232–5. doi: https://doi.org/10.1111/jicd.12232
2. Van Dessel J, Nicolielo LFP, Huang Y, Slagmolen P, Politis C, Lambrichts I, et al. Quantification of bone quality using different cone beam computed tomography devices: accuracy assessment for edentulous human mandibles. *Eur J Oral Implantol* 2017; **9**: 411–24Pubmed; PMID.
3. Jacobs R, Salmon B, Codari M, Hassan B, Bornstein MM. Cone beam computed tomography in implant dentistry: recommendations for clinical use. *BMC Oral Health* 2018; **18**: 1–16. doi: https://doi.org/10.1186/s12903-018-0523-5
4. Parsa A, Ibrahim N, Hassan B, Motroni A, van der Stelt P, Wismeijer D. Reliability of voxel gray values in cone beam computed tomography for preoperative implant planning assessment. *Int J Oral Maxillofac Implants* 2012; **27**: 1438–42.
5. Oliveira ML, Freitas DQ, Ambrosano GMB, Haiter-Neto F. Influence of exposure factors on the variability of CBCT voxel values: a phantom study. *Dentomaxillofac Radiol* 2014; **43**: 20140128. doi: https://doi.org/10.1259/dmfr.20140128
6. Pauwels R, Jacobs R, Singer SR, Mupparapu M. CBCT-based bone quality assessment: are Hounsfield units applicable? *Dento-*

maxillofac Radiol 2015; **44**: 20140238. doi: https://doi.org/10.1259/dmfr.20140238
7. Schulze R, Heil U, Gross D, Bruellmann DD, Dranischnikow E, Schwanecke U, et al. Artefacts in CBCT: a review. *Dentomaxillofac Radiol* 2011; **40**: 265–73. doi: https://doi.org/10.1259/dmfr/30642039
8. Spin-Neto R, Mudrak J, Matzen LH, Christensen J, Gotfredsen E, Wenzel A. Cone beam CT image artefacts related to head motion simulated by a robot skull: visual characteristics and impact on image quality. *Dentomaxillofac Radiol* 2013; **42**: 32310645. doi: https://doi.org/10.1259/dmfr/32310645
9. Vasconcelos KF, Nicolielo LFP, Nascimento MC, Haiter-Neto F, Bóscolo FN, Van Dessel J, et al. Artefact expression associated with several cone-beam computed tomographic machines when imaging root filled teeth. *Int Endod J* 2015; **48**: 994–1000. doi: https://doi.org/10.1111/iej.12395
10. Codari M, de Faria Vasconcelos K, Haiter Neto F, Jacobs R. Quantitative evaluation of metal artifacts using different CBCT devices, high-density materials and field of views. *Clin Oral Implants Res* 2017;: 1–6.
11. Cremonini CC, Dumas M, Pannuti CM, Neto JBC, Cavalcanti MGP, Lima LA. Assessment of linear measurements of bone for implant sites in the presence of metallic artefacts using cone beam computed tomography and multislice computed tomography. *Int J Oral Maxillofac Surg* 2011; **40**: 845–50. doi: https://doi.org/10.1016/j.ijom.2011.04.015
12. Fakhar HB, Rashtchian R, Parvin M. Effect of dental implant metal artifacts on accuracy of linear measurements by two cone-beam computed tomography systems before and after crown restoration. *J Dent* 2017; **14**: 329–36.
13. Bechara BB, Moore WS, McMahan CA, Noujeim M. Metal artefact reduction with cone beam CT: an in vitro study. *Dentomaxillofac Radiol* 2012; **41**: 248–53. doi: https://doi.org/10.1259/dmfr/80899839
14. Queiroz PM, Oliveira ML, Groppo FC, Haiter-Neto F, Freitas DQ. Evaluation of metal artefact reduction in cone-beam computed tomography images of different dental materials. *Clin Oral Investig* 2018; **22**: 419–23. doi: https://doi.org/10.1007/s00784-017-2128-9
15. Vasconcelos KdeF, Codari M, Queiroz PM, Nicolielo LFP, Freitas DQ, Sforza C, et al. The performance of metal artifact reduction algorithms in cone beam computed tomography images considering the effects of materials, metal positions, and fields of view. *Oral Surg Oral Med Oral Pathol Oral Radiol* 2019; **127**: 1–6. doi: https://doi.org/10.1016/j.oooo.2018.09.004
16. Gerlach NL, Meijer GJ, Borstlap WA, Bronkhorst EM, Bergé SJ, Maal TJJ. Accuracy of bone surface size and cortical layer thickness measurements using cone beam computerized tomography. *Clin Oral Implants Res* 2013; **24**: 793–7. doi: https://doi.org/10.1111/j.1600-0501.2012.02459.x
17. Parsa A, Ibrahim N, Hassan B, van der Stelt P, Wismeijer D. Bone quality evaluation at dental implant site using multislice CT, micro-CT, and cone beam CT. *Clin Oral Implants Res* 2015; **26**: e1–7. doi: https://doi.org/10.1111/clr.12315
18. Dau M, Edalatpour A, Schulze R, Al-Nawas B, Alshihri A, Kämmerer PW. Presurgical evaluation of bony implant sites using panoramic radiography and cone beam computed tomography-influence of medical education. *Dentomaxillofac Radiol* 2017; **46**: 20160081. doi: https://doi.org/10.1259/dmfr.20160081
19. Bamba J, Araki K, Endo A, Okano T. Image quality assessment of three cone beam CT machines using the SEDENTEXCT CT phantom. *Dentomaxillofac Radiol* 2013; **42**: 20120445. doi: https://doi.org/10.1259/dmfr.20120445
20. de Oliveira MVL, Wenzel A, Campos PSF, Spin-Neto R. Quality assurance phantoms for cone beam computed tomography: a systematic literature review. *Dentomaxillofac Radiol* 2017; **46**: 20160329. doi: https://doi.org/10.1259/dmfr.20160329
21. Steiding C, Kolditz D, Kalender WA. A quality assurance framework for the fully automated and objective evaluation of image quality in cone-beam computed tomography. *Med Phys* 2014; **41**: 031901. doi: https://doi.org/10.1118/1.4863507
22. Yamaguto OT, Vasconcelos MHF. Determinação das medidas dentárias mésio-distais em indivíduos brasileiros leucodermas com oclusão normal. *Rev. Dent. Press Ortodon. Ortop. Facial* 2005; **10**: 99–107. doi: https://doi.org/10.1590/S1415-54192005000500010
23. Sousa MVS, Vasconcelos EC, Janson G, Garib D, Pinzan A. Accuracy and reproducibility of 3-dimensional digital model measurements. *Am J Orthod Dentofacial Orthop* 2012; **142**: 269–73. doi: https://doi.org/10.1016/j.ajodo.2011.12.028
24. Queiroz PM, Santaella GM, Capelozza ALA, Rosalen PL, Freitas DQ, Haiter-Neto F. Zoom reconstruction tool: evaluation of image quality and influence on the diagnosis of root fracture. *J Endod* 2018; **44**: 621–5. doi: https://doi.org/10.1016/j.joen.2017.10.011
25. Fontenele RC, Nascimento EH, Vasconcelos TV, Noujeim M, Freitas DQ. Magnitude of cone beam CT image artifacts related to zirconium and titanium implants: impact on image quality. *Dentomaxillofac Radiol* 2018; **47**: 20180021. doi: https://doi.org/10.1259/dmfr.20180021
26. Freitas DQ, Fontenele RC, Nascimento EHL, Vasconcelos TV, Noujeim M. Influence of acquisition parameters on the magnitude of cone beam computed tomography artifacts. *Dentomaxillofac Radiol* 2018; **47**: 20180151. doi: https://doi.org/10.1259/dmfr.20180151
27. Machado AH, Fardim KAC, de Souza CF, Sotto-Maior BS, Assis NMSP, Devito KL. Effect of anatomical region on the formation of metal artefacts produced by dental implants in cone beam computed tomographic images. *Dentomaxillofac Radiol* 2018; **47**: 20170281. doi: https://doi.org/10.1259/dmfr.20170281
28. Molteni R. Prospects and challenges of rendering tissue density in Hounsfield units for cone beam computed tomography. *Oral Surg Oral Med Oral Pathol Oral Radiol* 2013; **116**: 105–19. doi: https://doi.org/10.1016/j.oooo.2013.04.013
29. Fokas G, Vaughn VM, Scarfe WC, Bornstein MM. Accuracy of linear measurements on CBCT images related to presurgical implant treatment planning: a systematic review. *Clin Oral Implants Res* 2018; **29 Suppl 16**: 393–415. doi: https://doi.org/10.1111/clr.13142
30. Bechara B, McMahan CA, Geha H, Noujeim M. Evaluation of a cone beam CT artefact reduction algorithm. *Dentomaxillofac Radiol* 2012; **41**: 422–8. doi: https://doi.org/10.1259/dmfr/43691321